

Dose Mapping After Endoradiotherapy with ^{177}Lu -DOTATATE/DOTATOC by a Single Measurement After 4 Days

Heribert Hänscheid¹, Constantin Lapa¹, Andreas K. Buck¹, Michael Lassmann¹, and Rudolf A. Werner^{1,2}

¹Department of Nuclear Medicine, University Hospital Würzburg, Würzburg, Germany; and ²Division of Nuclear Medicine and Molecular Imaging, The Russell H. Morgan Department of Radiology and Radiological Science, Johns Hopkins School of Medicine, Baltimore, Maryland

Peptide receptor radionuclide therapy (PRRT) using ^{177}Lu -DOTATATE/DOTATOC enables delivery of β -radiation to tumors with high expression of somatostatin receptors. Before the recent publication of the first data from a randomized, controlled, prospective study (NETTER-1) (1), nonrandomized observational studies had already demonstrated the superior overall benefit of PRRT (2–4). NETTER-1 has now confirmed these data, showing that treatment with ^{177}Lu -DOTATATE resulted in markedly longer progression-free survival and a significantly higher response rate than high-dose octreotide alone among patients with advanced midgut neuroendocrine tumors (1). Rising numbers of PRRT are already foreseeable.

The currently routinely used medium-energy γ -/ β -emitting nuclide ^{177}Lu opens the window for posttherapeutic scintigraphy as well as pretreatment dosimetry (5). The assessment of absorbed doses to tumors and organs can be used to estimate the therapeutic effect to the target tissue and to reduce side effects to critical organs, such as bone marrow or kidneys (5–8).

Although there is evidence that individually tailored treatment accurately planned by dosimetry is advantageous for PRRT optimization (8–10), standard activities are usually administered in a series of treatment cycles. The 1-size-fits-all concept of administering a fixed activity of 7.4 GBq, as used in the NETTER-1 trial, is covered by the recent practical guidance of the European Association of Nuclear Medicine (5). The cumulated absorbed dose to the kidneys, which often are the organs at risk in endoradiotherapy of NET, should not exceed predefined limits in a series of PRRT cycles. Dose verification after each PRRT cycle is therefore desirable to ensure safety and to assess the tumor dose indicating treatment efficacy (11). However, repeated measurements of the activities retained in assessed tissues over several days and an elaborate data evaluation are necessary for an exact dosimetry (12,13). The procedures require several patient visits and result in additional burdens. Noncompliance with procedural instructions, the complexity of dosimetry data interpretation, and flaws of routinely key data recording as part of clinical processes are main factors that are related to low performance rates of PRRT dosimetry studies (14). Attempts to find methods to reduce the efforts for data collection and dosimetry are desirable and have already been performed (15,16).

Aiming at a simplified dosimetry, which is well founded by a theoretic approach, we analyzed the accuracy of an absorbed dose estimate based on a single measurement of the activity retention.

For correspondence or reprints contact: Heribert Hänscheid, Department of Nuclear Medicine, University Hospital Würzburg, Oberdürrbacher Strasse 6, 97080 Würzburg, Germany.
E-mail: haenscheid_h@ukw.de

MATERIALS AND METHODS

Study Design

This study comprises a retrospective analysis of the activity kinetics in organs and tumors after ^{177}Lu -DOTATATE/DOTATOC from routinely acquired patient data. Included patients gave written informed consent for the recording and anonymized analysis of their data. The local ethics committee waived the need for further approval.

Patient Measurements

Activity kinetics were analyzed in the kidneys (excluding renal pelvis), livers, spleens, and in up to 2 NET lesions in patients who underwent ^{177}Lu -DOTATATE/DOTATOC. The first assessment for each patient with at least 4 planar whole-body scans, including measurements after 1–4 h, 1 d, 2 d, and 4 d or more after the activity administration, was analyzed. Data from 29 patients (17 women, 12 men) with histologically proven NET ($n = 21$) or meningioma ($n = 8$) who underwent PRRT at our institution between March 2010 and October 2016 were included. Patients underwent ^{177}Lu -DOTATATE ($n = 22$) or ^{177}Lu -DOTATOC ($n = 7$) for pretherapeutic dosimetry ($n = 7$; 164–225 MBq of ^{177}Lu) or treatment ($n = 22$; 5.3–8.1 GBq of ^{177}Lu). Only organ but not tumor kinetics were analyzed in the 8 patients with meningioma because the meningiomas showed significantly different activity kinetics as compared with NET lesions, in particular a shorter effective half-life.

Measurements were performed with dual head γ -cameras (DUET or Symbia; Siemens) equipped with medium-energy collimators. All whole-body scans in a series were acquired using the same camera and identical camera settings (matrix, $1,024 \times 256$; 20% window at 208 keV; identical measuring distance). Regions of interest were drawn including the organ or NET lesion, or part of the tissue in the case of overlapping accumulating tissues, under consideration and over an area with representative background. Identical regions were copied to each scan in the series, and background-corrected counting rates were extracted. Organs completely masked by uptake in other tissues were considered unmeasurable and were excluded from further analyses. The images were not corrected for attenuation and scatter because attenuation maps and triple-energy data were not available for most of the routinely acquired whole-body scans. Activities in the regions of interest were not quantified; only the temporal development of the counting rates was determined assuming identical attenuation, scatter, and sensitivity in all scans in a series.

Theory and Data Evaluation

A biexponential decay function was fitted to the counting rate kinetics of each measurable organ or tumor by ordinary least-squares regression, and the Pearson correlation coefficient r was calculated. Some tissues showed a monoexponential decay function, which was adopted if the correspondent fit resulted in an r greater than 0.98. The fit functions of 54 kidneys, 25 livers, 27 spleens, and 30 NET lesions were included in further analysis. Each fit function was normalized to 100% at its maximum to deduce the normalized uptake function $u(r_s, t)$, where r_s denotes the tissue under consideration and t the time after the administration. Figure 1 shows, as an example, the functions $u(r_s, t)$ of the kidneys in a patient with meningioma.

The total absorbed dose $D(r_s)$ to r_s by self-irradiation is (17):

$$D(r_s) = \int_{t=0}^{\infty} A(r_s, t) \times S(r_s \leftarrow r_s) dt, \quad \text{Eq. 1}$$

where $A(r_s, t)$ is the activity time function and $S(r_s \leftarrow r_s)$ the dose rate per unit activity in r_s . $A(r_s, t)$ can be deduced from $u(r_s, t)$ when the absolute activity $A(r_s, t_1)$ at any given time t_1 is known from a quantitative assessment:

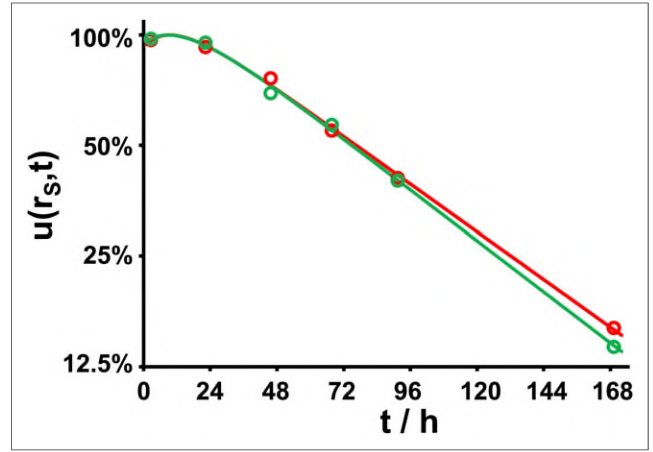


FIGURE 1. Normalized uptake in left (red; $u(r_s, t) = 129.8\%/2^{t/55.6\text{ h}} - 37.2\%/2^{t/7.4\text{ h}}$) and right (green; $u(r_s, t) = 136.0\%/2^{t/52.0\text{ h}} - 41.2\%/2^{t/9.0\text{ h}}$) kidneys of patient with meningioma after administration of 7 GBq of ^{177}Lu -DOTATATE.

$$A(r_s, t) = u(r_s, t) \times \frac{A(r_s, t_1)}{u(r_s, t_1)}. \quad \text{Eq. 2}$$

Equation 1 becomes:

$$D(r_s) = \frac{A(r_s, t_1)}{u(r_s, t_1)} \times S(r_s \leftarrow r_s) \times \tilde{u}(r_s), \quad \text{Eq. 3}$$

with $\tilde{u}(r_s)$ representing the time integral of $u(r_s, t)$:

$$\tilde{u}(r_s) = \int_{t=0}^{\infty} u(r_s, t) dt. \quad \text{Eq. 4}$$

The time integral of a function $u(r_s, t) = u(r_s, 0) \times 2^{-t/T_{\text{eff}}}$ decaying monoexponentially with an effective half-life T_{eff} is $\tilde{u}(r_s) = u(r_s, 0) \times T_{\text{eff}}/\ln(2)$. $\tilde{u}(r_s)$ is related to the uptake $u(r_s, t_1) = u(r_s, 0) \times 2^{-t_1/T_{\text{eff}}}$ after time t_1 by:

$$\tilde{u}(r_s) = u(r_s, t_1) \times \frac{2^{t_1/T_{\text{eff}}} \times T_{\text{eff}}}{\ln(2)}. \quad \text{Eq. 5}$$

Within a certain time interval after the activity administration, which is determined by the value of T_{eff} , the factor $2^{t_1/T_{\text{eff}}} \times T_{\text{eff}}$ in Equation 5 can be approximated by the factor $2 \times t_1$ (18,19) with less than 10% deviation for $0.75 < t_1/T_{\text{eff}} < 2.5$ (Fig. 2). The time integral $\tilde{u}(r_s)$ of a monoexponential decay function can therefore be estimated from only a single measurement at time t_1 by the approximation $\tilde{u}_1(r_s, t_1)$:

$$\tilde{u}(r_s) \approx \tilde{u}_1(r_s, t_1) = u(r_s, t_1) \times \frac{2 \times t_1}{\ln(2)}. \quad \text{Eq. 6}$$

In PRRT, however, the fit functions $u(r_s, t)$ are often biexponential (12,16,20). To investigate whether the approximation in Equation 6 can nonetheless be used to estimate absorbed doses in PRRT with an acceptable uncertainty from a single measurement, the expected $u(r_s, t_1)$ at $t_1 = 24, 48, 72, 96, 120,$ and 144 h were calculated for each uptake function and used to determine the error introduced by the approximation.

When Equations 3 and 6 are combined, the absorbed dose is approximated with the present approach by:

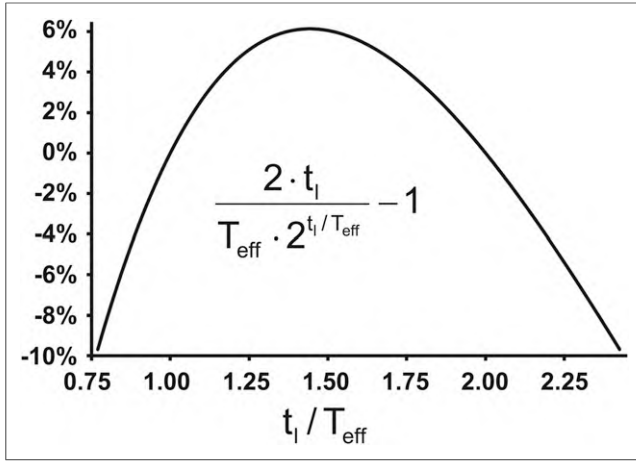


FIGURE 2. Deviation of ratio of $2 \times t_1$ and the factor $T_{\text{eff}} \times 2^{t_1/T_{\text{eff}}}$ from unity in time interval $0.75 \times T_{\text{eff}} < t_1 < 2.5 \times T_{\text{eff}}$.

$$D(r_S) \approx A(r_S, t_1) \times S(r_S \leftarrow r_S) \times \frac{2 \times t_1}{\ln(2)}. \quad \text{Eq. 7}$$

RESULTS

Normalized Uptake Functions $u(r_S, t)$

The correlation coefficient r exceeded 0.98 in monoexponential fits in 25 of 54 kidneys, 12 of 25 livers, 3 of 27 spleens, and 7 of 22 tumors. Biexponential functions $u(r_S, t)$ were assumed for the remaining tissues. The biexponential functions generally showed a dominant component, with longer effective half-life and a short-lived component leading to some deviation from a monoexponential decay shortly after the administration. Compared with the time integral of the main component, the time integral of the short-lived component was a median of -5% (range, -17% to -1%) in kidneys, -2% (range, -5% to $+7\%$) in livers, -3% (range, -14% to -1%) in spleens, and -2% (range, -10% to 0%) in tumors. The tissue-specific effective half-life of the main component in all evaluated tissues was a median of 51 h (range, 40–68 h with 1 outlier at 106 h) in kidneys, 67 h (range, 55–117 h) in livers, 68 h (range, 52–99 h) in spleens, and 77 h (range, 56–130 h) in tumors.

Error of Single Sample Estimates

Table 1 shows the observed empiric correlation between the approximation $\tilde{u}_1(r_S, t_1)$ and the time integral $\tilde{u}(r_S)$. The Pearson correlation coefficient improved with increasing time t_1 . A strong linear relationship between $\tilde{u}_1(r_S, t_1)$ and $\tilde{u}(r_S)$ was observed only at late times t_1 , indicating that estimates based on early measurements are less reliable.

Figure 3 shows the error introduced by the approximation in Equation 6 in dependence on the actual time integral $\tilde{u}(r_S)$ for all evaluated tissues. The error is defined as the percentage deviation of the ratio $\tilde{u}_1(r_S, t_1)/\tilde{u}(r_S)$ from unity. Data points that originate from monoexponential decay functions are located on the gray lines (Fig. 3). Deviations of data points from the gray lines are due to the influence of a second short lived component. Quantiles of the distribution of deviations are listed in Table 2.

The kidneys, which most often represent the dose-limiting organs and typically showed the shortest effective half-life, T_{eff} , were best represented by approximations based on the

TABLE 1

Correlation Between Approximation $\tilde{u}_1(r_S, t_1) = u(r_S, t_1) \times 2 \times t_1 / \ln(2)$ Deduced from Single Measurement After 24, 48, 72, 96, 120, and 144 Hours and Actual Time Integral $\tilde{u}(r_S)$

Tissue	Pearson correlation coefficient r					
	24 h	48 h	72 h	96 h	120 h	144 h
Kidneys	0.73	0.84	0.93	0.98	0.99	0.98
Liver	0.67	0.84	0.93	0.98	0.99	0.99
Spleen	0.55	0.77	0.89	0.97	0.99	0.99
NET	0.63	0.80	0.92	0.97	0.99	0.99

measurements after 72 and 96 h. For the 96-h values, deviation was a median of $+5\%$, with underestimates of more than 5% (-9% both) in only 2 of 54 kidneys (1 patient) and overestimates of more than 10% (up to 17%) in 6 kidneys (4 patients). The measurement at 120 h was superior for livers, spleens, and tumors, which typically showed longer effective half-lives.

The approximation in Equation 6 is inadequate for measurements after 24 h, which generally led to unacceptable underestimates of absorbed doses in all tissues. Large underestimates were also observed for measurements after 48 h in tissues with a long effective half-life and for 144 h in those with short half-life.

The approximation based on the 96-h measurement provided good agreement for all tissues. The median deviation for all organs and NET lesions was $+6\%$ (range, -11% to $+20\%$), and 90% of deviations ranged between -4% and $+15\%$.

DISCUSSION

The method presented in this work is a potential option to deduce an estimate of the absorbed doses in abdominal organs and NET lesions from a single late-activity measurement. It is not based on an empirically observed correlation, but rather provides an approximation that is well substantiated by theory when an adequate time of measurement is selected and the decay function shows only minor deviations from a monoexponential decay.

Time of Measurement

The error introduced by the approximation is limited to the deviations shown in Figure 2 for tissues with activities decaying monoexponentially. Figure 4 shows the time window for a reliable dose estimate in such tissues for different effective half-lives. Underestimates of the actually absorbed dose exceeding 10% occur only if the ratio t_1/T_{eff} is smaller than 0.75 or larger than 2.5. A measurement at $t_1 = 96$ h opens a window for reliable single-sample dosimetry for effective half-lives ranging from 38 to 128 h. In the present investigation, all tissues but 1 NET lesion ($T_{\text{eff}} = 130$ h) met this requirement.

Especially absorbed doses in kidneys, which most often represent the dose-limiting organ in PRRT with ^{177}Lu -DOTATATE/DOTATOC, must not be significantly underestimated by any dose approximation. Half-lives of the main decay component in kidneys were a median of 51 h and ranged from 40 to 68 h with 1 outlier at 106 h in a patient with only 1 kidney. These data are consistent to those reported by others (15,21). Given the actually observed half-lives, a measurement at $t_1 = 72$ h, which induces less than

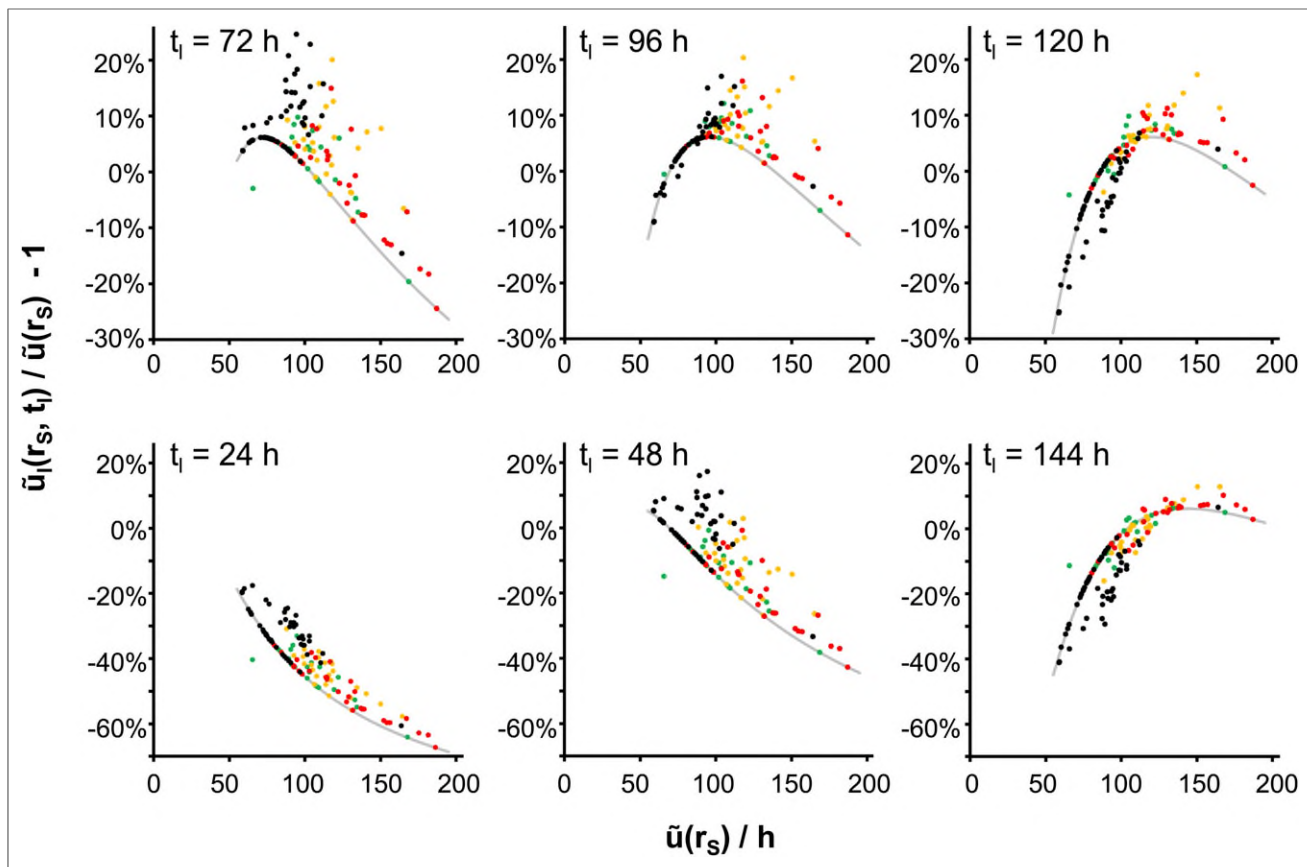


FIGURE 3. Percentage deviation of approximation $\bar{u}_i(r_s, t_i) = u(r_s, t_i) \times 2 \times t_i / \ln(2)$ from $\bar{u}(r_s)$ vs. actual time integral $\bar{u}(r_s)$ for single measurements after $t_i = 72, 96,$ and 120 h (top; scale, -30% to 25%) and $t_i = 24, 48,$ and 144 h (bottom; scale, -70% to 25%). Deviations are positive for overestimations and negative for underestimations of actually absorbed doses. Each point represents kidney (black), liver (green), spleen (yellow), or NET lesion (red). Gray line shows deviation expected for monoexponential decay functions.

10% error for $29 < T_{\text{eff}} < 96$ h, is also adequate for kidneys. However, the absorbed dose for the outlier at 106 h was underestimated by the 72-h uptake by 15%. Approximations based on earlier measurements led to an increased risk for higher deviations and a reduced correlation between dose estimates and actual doses. This finding is in agreement with the observation by Miederer et al. (16) that the correlation between the absorbed dose from PRRT with ^{177}Lu and the kidney uptake measured in OctreoScan improved with increasing time of measurement.

Effective half-lives in livers, spleens, and NET lesions ranged from 52 to 130 h. Measurement should be performed after 96 or after 120 h ($<10\%$ error for $48 < T_{\text{eff}} < 160$ h) for these tissues.

Decay Functions

Most tissues evaluated in the present investigation showed a biexponential decay function. Consideration of potential deviations from a monoexponential decay is not uniform in PRRT dosimetry. Most often, any short-lived component is ignored (8,9,15,22–26), as is also the case with the single-sample approximation. A second decay component early after the activity administration can induce both over- and underestimates depending on its time integral in comparison to the time integral of the dominant long-lived component. Only few biexponential functions in our study showed biphasic clearance, with 2 components

with positive amplitude. In most cases, a negative short-lived component was observed, indicating further accumulation early after the activity administration, as visible in the example shown in Figure 1. Such a negative component leads to an overestimation of the absorbed dose by the single-sample approximation. The contribution by the short-lived component in functions with biphasic clearance was generally too small to produce a considerable dose underestimate.

Uncertainties

Guerrero et al. (20) have analyzed the impacts of timing of measurements and the time–activity integration method. The authors found that these parameters strongly influenced the dosimetric calculations and that only a few measurements up to 4 d were often not sufficient for a uniquely defined fit of the activity time function. This was observable in the present study also; biexponential fitting often resulted in parameters with high uncertainty and covariance. The uncertainties can be reduced with later measurements. Heikkonen et al. (15), neglecting the effect of the short-lived component, acquired the last measurement after 168 h and reported a high correlation between simplified dosimetry from 2 measurements after 24 and 168 h and full dosimetry with an additional scan after 72 h. For highest accuracy, larger numbers of measurements especially during the first day and after a week or later after the activity administration would be desirable.

TABLE 2

Median, Range, and 0.1 and 0.9 Quantiles of Percentage Deviation of Approximation $\tilde{u}_i(r_S, t_i) = u(r_S, t_i) \times 2 \times t_i / \ln(2)$ Deduced from Single Measurement after 24, 48, 72, 96, 120, and 144 Hours from Actual Time Integral $\tilde{u}(r_S)$

Tissue	Quantile	$\tilde{u}_i(r_S, t_i) / \tilde{u}(r_S) - 1$					
		24 h	48 h	72 h	96 h	120 h	144 h
Kidneys	1 (maximum)	-18%	+17%	+ 25%	+17%	+7%	+7%
	0.9	-24%	+9%	+16%	+10%	+2%	-7%
	0.5 (median)	-33%	0%	+6%	+5%	-5%	-18%
	0.1	-40%	-8%	+4%	-3%	-16%	-31%
	0 (minimum)	-61%	-33%	-15%	-9%	-25%	-41%
Liver	1 (maximum)	-33%	-1%	+10%	+12%	+10%	+6%
	0.9	-37%	-6%	+7%	+9%	+8%	+5%
	0.5 (median)	-43%	-11%	+4%	+6%	+3%	-1%
	0.1	-52%	-21%	-4%	+3%	-1%	-11%
	0 (minimum)	-64%	-38%	-20%	-7%	-4%	-12%
Spleen	1 (maximum)	-31%	+3%	+20%	+20%	+17%	+13%
	0.9	-38%	-2%	+12%	+15%	+12%	+8%
	0.5 (median)	-44%	-12%	+5%	+8%	+6%	+1%
	0.1	-53%	-22%	-4%	+5%	+3%	-7%
	0 (minimum)	-58%	-27%	-9%	+2%	-4%	-16%
NET	1 (maximum)	-36%	-1%	+15%	+16%	+11%	+10%
	0.9	-40%	-6%	+8%	+10%	+10%	+7%
	0.5 (median)	-49%	-17%	0%	+6%	+5%	+5%
	0.1	-60%	-32%	-13%	-2%	+2%	-6%
	0 (minimum)	-67%	-43%	-24%	-11%	-3%	-14%

Kinetics were determined from counting rates observed in organ and background regions in planar images without correction for attenuation and scatter. The background and its change in time can be different in such regions, especially in the presence of overlapping tissues or variable intestinal activity, leading to a modification of the $u(r_S, t)$ function and thus the time integral $\tilde{u}(r_S)$. Uncertainties would have been smaller for kinetics deduced from series of SPECT measurements.

It is, therefore, a shortcoming of the present study that the normalized uptake functions $u(r_S, t)$ measured in the present study cannot be considered to be a gold standard reflecting the true kinetics with negligible error, although the accuracy of the approximation is not sensitive to the exact values of the fit parameters in $u(r_S, t)$. However, independent verification of the methodology in other patient groups is necessary before routine application.

Advantages of Single-Sample Dosimetry

The single-sample method enables dose estimates with even lower expense than earlier methods to simplify dosimetry. Our study indicates that it provides absorbed dose data with only minor additional errors compared with full dosimetry, thus enabling routinely performed dosimetry during each PRRT cycle with little additional effort.

In principle, activity data extracted from a single planar scan after 96 h can be used to approximate the absorbed dose. Most reports of absorbed doses from PRRT are based on planar imaging and conjugate-view activity quantification (13). However,

accuracy of dosimetry from planar scans is limited, and large systematic errors are possible even after careful correction of background, scatter, and attenuation (13,22,25,27).

Any potential error from inadequate background or attenuation correction of planar images as well as unsuitable fitting and

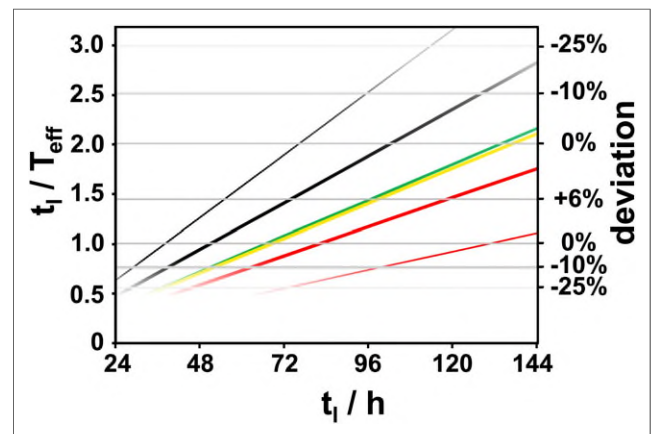


FIGURE 4. Ratio t_i / T_{eff} and deviation of ratio of $2 \times t_i$ and the factor $T_{\text{eff}} \times 2^{t_i / T_{\text{eff}}}$ from unity in dependence on time of measurement t_i for monoexponential decay functions. Lines represent median effective half-lives of main component in kidneys (black bold), livers (green), spleens (yellow), and NET lesions (red bold) as well as shortest (black thin) and longest (red thin) measured half-life.

integration of $u(r_s, t)$ due to insufficient data acquisition are excluded when the single-sample method is used together with high-quality SPECT/CT imaging with state-of-the-art quantitative reconstruction and partial-volume correction. Phantom measurements indicate that the activity concentration can be quantified by SPECT/CT with ^{177}Lu with uncertainties of 10% or less (13,28).

It is an inherent benefit of the method that the absorbed dose estimate is largely independent of the effective half-life. While even skillful planar dosimetry with several measurements is usually unsuitable to identify differences in kinetics and absorbed doses in distinct areas of organs or tumors, an approximation based on a late quantitative SPECT/CT correctly reproduces the inhomogeneity of the distribution of absorbed doses. The counting rate information in the reconstructed SPECT images is proportional to the absorbed doses. Thus, apart from image distortion inherently present in SPECT, such as partial-volume effects, the data represent a 3-dimensional approximation of the dose distribution.

Dosimetric Procedure

Information on the best practice to produce reliable quantitative SPECT data for ^{177}Lu were described by Ljungberg et al. (13). After patient imaging and quantitative SPECT data reconstruction, the counts in a volume of interest large enough to avoid major reconstruction errors were, with reasonable accuracy, proportional to the absorbed doses approximated by Equation 7. The product $S(r_s \leftarrow r_s) \times 2/\ln(2)$ in Equation 7 is almost inversely proportional to the size of the tissue. It can be determined with the sphere model in OLINDA/EXM (29) that a constant factor of $m \times S(r_s \leftarrow r_s) \times 2/\ln(2) = 0.25 \text{ Gy}\cdot\text{g}/\text{MBq}\cdot\text{h}$ ($\pm 2\%$) is valid for accumulating tissues with masses m between 10 g and 1 kg. The activity concentration in a volume of interest within such a tissue can be calculated from the counts C_{VOI} and the mass m_{VOI} in that volume, the sensitivity of the γ -camera ϵ (13), and the total acquisition duration t_{acq} (frame duration times number of angular steps). The absorbed dose becomes:

$$D(r_s) \approx A(r_s, t_1) \times S(r_s \leftarrow r_s) \times \frac{2 \times t_1}{\ln(2)} = 0.25 \frac{\text{Gy}\cdot\text{g}}{\text{MBq}\cdot\text{h}} \times \frac{C_{\text{VOI}} \cdot t_1}{t_{\text{acq}} \cdot m_{\text{VOI}} \cdot \epsilon} \quad \text{Eq. 8}$$

The following example uses arbitrary values: a double-head γ -camera has a sensitivity of 10 cps/MBq per head ($\epsilon = 20 \text{ cps}/\text{MBq}$). SPECT is acquired with 60 angular steps (120 projections) and 20-s acquisition duration per angular step ($t_{\text{acq}} = 60 \times 20 \text{ s} = 1,200 \text{ s}$). According to Equation 8, the absorbed dose in a volume of interest with 40 g of healthy liver tissue with 84,000 counts in an acquisition at $t_1 = 92 \text{ h}$ after PRRT is 2 Gy.

CONCLUSION

The absorbed dose from PRRT with ^{177}Lu to NET lesions and relevant abdominal organs can be deduced with reasonable accuracy from a single measurement 4 d after the activity administration by an approximation, which is substantiated by theory. All ^{177}Lu -accumulating tissues showing monoexponential decay with effective half-lives between 38 and 128 h are well represented, with an error of less than 10%. Deviations

from a monoexponential decay function, which most often are not considered in PRRT dosimetry due to a lack of data points, potentially induce additional errors.

The method to approximate absorbed doses from counting rates obtained by quantitative SPECT/CT imaging is easy to implement, provides a 3-dimensional dose map, and is a promising option to register cumulated doses actually absorbed in a series of PRRT treatment cycles with minor additional resources and effort.

DISCLOSURE

No potential conflict of interest relevant to this article was reported.

REFERENCES

1. Strosberg J, El-Haddad G, Wolin E, et al. Phase 3 trial of ^{177}Lu -Dotatate for midgut neuroendocrine tumors. *N Engl J Med*. 2017;376:125–135.
2. Kwekkeboom DJ, de Herder WW, Kam BL, et al. Treatment with the radiolabeled somatostatin analog [^{177}Lu -DOTA 0,Tyr3]octreotate: toxicity, efficacy, and survival. *J Clin Oncol*. 2008;26:2124–2130.
3. Baum RP, Kluge AW, Kulkarni H, et al. [^{177}Lu -DOTA](0)-D-Phe(1)-Tyr(3)-Octreotide (^{177}Lu -DOTATOC) for peptide receptor radiotherapy in patients with advanced neuroendocrine tumours: a phase-II study. *Theranostics*. 2016;6:501–510.
4. Sabet A, Dautzenberg K, Haslerud T, et al. Specific efficacy of peptide receptor radionuclide therapy with ^{177}Lu -octreotate in advanced neuroendocrine tumours of the small intestine. *Eur J Nucl Med Mol Imaging*. 2015;42:1238–1246.
5. Bodei L, Mueller-Brand J, Baum RP, et al. The joint IAEA, EANM, and SNMMI practical guidance on peptide receptor radionuclide therapy (PRRT) in neuroendocrine tumours. *Eur J Nucl Med Mol Imaging*. 2013;40:800–816.
6. Werner RA, Beykan S, Higuchi T, et al. The impact of ^{177}Lu -octreotide therapy on $^{99\text{m}}\text{Tc}$ -MAG3 clearance is not predictive for late nephropathy. *Oncotarget*. 2016;7:41233–41241.
7. Sabet A, Ezziddin K, Pape UF, et al. Long-term hematotoxicity after peptide receptor radionuclide therapy with ^{177}Lu -octreotate. *J Nucl Med*. 2013;54:1857–1861.
8. Sandström M, Garske-Roman U, Granberg D, et al. Individualized dosimetry of kidney and bone marrow in patients undergoing ^{177}Lu -DOTA-octreotate treatment. *J Nucl Med*. 2013;54:33–41.
9. Svensson J, Berg G, Wangberg B, Larsson M, Forssell-Aronsson E, Bernhardt P. Renal function affects absorbed dose to the kidneys and haematological toxicity during ^{177}Lu -DOTATATE treatment. *Eur J Nucl Med Mol Imaging*. 2015;42:947–955.
10. Svensson J, Hagmarker L, Magnander T, Wangberg B, Bernhardt P. Radiation exposure of the spleen during ^{177}Lu -DOTATATE treatment and its correlation with haematological toxicity and spleen volume. *EJNMMI Phys*. 2016;3:15.
11. *Practical Guidance on Peptide Receptor Radionuclide Therapy (PRRT) for Neuroendocrine Tumours*. Vienna, Austria: International Atomic Energy Agency; 2013.
12. Siegel JA, Thomas SR, Stubbs JB, et al. MIRD pamphlet no. 16: techniques for quantitative radiopharmaceutical biodistribution data acquisition and analysis for use in human radiation dose estimates. *J Nucl Med*. 1999;40:37S–61S.
13. Ljungberg M, Celler A, Konijnenberg MW, et al. MIRD pamphlet no. 26: joint EANM/MIRD guidelines for quantitative ^{177}Lu SPECT applied for dosimetry of radiopharmaceutical therapy. *J Nucl Med*. 2016;57:151–162.
14. Lassmann M, Strigari L, Bardies M. Dosimetry is alive and well. *Cancer Biother Radiopharm*. 2010;25:593–595.
15. Heikkonen J, Maenpää H, Hippeläinen E, Reijonen V, Tenhunen M. Effect of calculation method on kidney dosimetry in Lu-177-octreotate treatment. *Acta Oncol*. 2016;55:1069–1076.
16. Miederer M, Reber H, Helisch A, Fottner C, Weber M, Schreckenberger M. One single-time-point kidney uptake from OctreoScan correlates with number of desintegrations measured over 72 hours and calculated for the 6.7 hours half-life nuclide ^{177}Lu . *Clin Nucl Med*. 2012;37:e245–e248.

17. Bolch WE, Eckerman KF, Sgouros G, Thomas SR. MIRD pamphlet no. 21: a generalized schema for radiopharmaceutical dosimetry—standardization of nomenclature. *J Nucl Med.* 2009;50:477–484.
18. Hänscheid H, Lassmann M, Reiners C. Dosimetry prior to ¹³¹I-therapy of benign thyroid disease. *Z Med Phys.* 2011;21:250–257.
19. Hänscheid H, Canzi C, Eschner W, et al. EANM Dosimetry Committee series on standard operational procedures for pre-therapeutic dosimetry: II—dosimetry prior to radioiodine therapy of benign thyroid diseases. *Eur J Nucl Med Mol Imaging.* 2013;40:1126–1134.
20. Guerriero F, Ferrari ME, Botta F, et al. Kidney dosimetry in ¹⁷⁷Lu and ⁹⁰Y peptide receptor radionuclide therapy: influence of image timing, time-activity integration method, and risk factors. *BioMed Res Int.* 2013;2013:935351.
21. Garske U, Sandstrom M, Johansson S, et al. Minor changes in effective half-life during fractionated ¹⁷⁷Lu-Octreotate therapy. *Acta Oncol.* 2012;51:86–96.
22. Larsson M, Bernhardt P, Svensson JB, Wangberg B, Ahlman H, Forssell-Aronsson E. Estimation of absorbed dose to the kidneys in patients after treatment with ¹⁷⁷Lu-octreotate: comparison between methods based on planar scintigraphy. *EJNMMI Res.* 2012;2:49.
23. Baechler S, Hobbs RF, Boubaker A, et al. Three-dimensional radiobiological dosimetry of kidneys for treatment planning in peptide receptor radionuclide therapy. *Med Phys.* 2012;39:6118–6128.
24. Esser JP, Krenning EP, Teunissen JJM, et al. Comparison of [¹⁷⁷Lu-DOTA0, Tyr3]octreotate and [¹⁷⁷Lu-DOTA0, Tyr3]octreotide: which peptide is preferable for PRRT? *Eur J Nucl Med Mol Imaging.* 2006;33:1346–1351.
25. Sandström M, Garske U, Granberg D, Sundin A, Lundqvist H. Individualized dosimetry in patients undergoing therapy with ¹⁷⁷Lu-DOTA-D-Phe(1)-Tyr(3)-octreotate. *Eur J Nucl Med Mol Imaging.* 2010;37:212–225.
26. Bodei L, Cremonesi M, Ferrari M, et al. Long-term evaluation of renal toxicity after peptide receptor radionuclide therapy with ⁹⁰Y-DOTATOC and ¹⁷⁷Lu-DOTATATE: the role of associated risk factors. *Eur J Nucl Med Mol Imaging.* 2008;35:1847–1856.
27. Garkavij M, Nickel M, Sjogreen-Gleisner K, et al. ¹⁷⁷Lu-[DOTA0, Tyr3] Octreotate therapy in patients with disseminated neuroendocrine tumors: analysis of dosimetry with impact on future therapeutic strategy. *Cancer.* 2010;116:1084–1092.
28. Beauregard JM, Hofman MS, Pereira JM, Eu P, Hicks RJ. Quantitative ¹⁷⁷Lu SPECT (QSPECT) imaging using a commercially available SPECT/CT system. *Cancer Imaging.* 2011;11:56–66.
29. Stabin MG, Sparks RB, Crowe E. OLINDA/EXM: the second-generation personal computer software for internal dose assessment in nuclear medicine. *J Nucl Med.* 2005;46:1023–1027.